JOURNAL OF MATERIALS SCIENCE 18 (1983) 114–126

Superconductivity of Zr–Nb–Si amorphous alloys

A. INOUE, N. TOYOTA, T. FUKASE, T. MASUMOTO
The Research Institute for Iron, Steel and Other Metals, Sendai 980, Japan

Y. TAKAHASHI
Graduate School, Tohoku University, Sendai 980, Japan

Superconducting amorphous alloys with high strength and good ductility have been found in rapidly quenched alloys of the Zr–Nb–Si system. These alloys were produced in a continuous ribbon form of 1 to 2 mm width and 0.02 to 0.03 mm thickness using a modified single roller quenching apparatus. The amorphous alloys were formed over the whole composition range between zirconium and niobium, but the silicon content was limited to the relatively narrow range between about 12 and 24 at %. All the amorphous alloys showed a superconducting transition whose temperature, T_c, increased from 2.31 to 4.20 K with increasing niobium content or with decreasing silicon content. The upper critical magnetic field, H_{c2}, and the critical current density, J_c, for $Zr_{15}Nb_{70}Si_{15}$ alloy were of the order of 4.5 Tesla(T) and 5.5×10^6 A m^{-2} at 1.5 K in the absence of applied field. The upper critical field gradient at T_c, $(dH_{c2}/dT)_{T_c}$, and the electrical resistivity at 4.2 K, ρ_n, decreased from 2.89 to 2.10 T K^{-1} and from 2.70 to 1.80 $\mu\Omega$m, respectively, with the amount of niobium. The Debye temperature, θ_D, the electron-phonon coupling constant, λ, and the bare density of electronic states at the Fermi level, $N(E_f)$ were calculated from the experimentally measured values of ρ_n, $(dH_{c2}/dT)_{T_c}$, Young's modulus and density by using the strong-coupling theories. From the comparison of T_c with their calculated parameters, it was found that λ is the most dominant parameter for T_c. The GL parameter, κ, and the GL coherence length, $\xi_{GL}(0)$, were estimated to be 70 to 100 and about 7.6 nm, respectively, from the experimental values of $(dH_{c2}/dT)_{T_c}$ and ρ_n by using the GLAG theory and hence it is concluded that the present amorphous alloys are an extremely "dirty" type-II superconductor having a very weak flux pinning force.

1. Introduction

Crystalline alloys consisting of IV and V group transition metals (Ti, Zr, Hf, V, Nb and Ta) of the Periodic Table have been known to be considerably good superconductors and hence if these transition metal-based amorphous alloys are formed, it is expected that these alloys may exhibit good superconducting properties. Furthermore, in order to clarify the mechanism of the superconductivity of amorphous alloys, it is a very important research subject to compare the superconductivity and its related parameters of their alloys in the amorphous state with those in the crystalline state. Recently, the amorphous-phase formation of rapidly quenched (Zr, Hf)–V binary [1] and Ti–(V, Nb or Ta)–Si [2–4] and Hf–(V or Nb)–Si [5] ternary alloys has been reported in wide composition ranges. In addition, it has also been found that the Ti–Nb–Si amorphous alloys exhibit a superconducting transition above the liquid-helium temperature (4.2 K) [2], in addition to good thermal stability, high mechanical strength and ductile nature [5]. Considering the previous data on crystalline superconducting

0022–2461/83/010114–13$04.06/0

alloys, it was expected that the Zr–(V, Nb, or Ta)-based alloys might also exhibit rather good superconductivity in the amorphous state. The purpose of this paper is to examine the composition range for the formation of the amorphous phase in the Zr–Nb–Si system and the mechanical properties, thermal stability and superconducting properties of these amorphous alloys and to evaluate the dominating parameters for superconductivity in the amorphous alloys based on the BCS–GLAG [6] and strong coupling [7] theories for type-II superconductors.

2. Experimental methods

Zr–Nb–Si alloys of different compositions were pre-alloyed under a purified and gettered argon atmosphere in an arc furnace on a water-cooled copper mould from zirconium (99.6 wt%) containing 0.086 wt% O_2, 0.051 wt% Fe and 0.014 wt% Cr, etc., impurities, niobium (99.5 wt%) containing 0.085 wt% O_2, 0.078 wt% Ta and 0.008 wt% C, etc., impurities, and silicon (99.999 wt%). The weight of the mixture melted in one run was about 30 g. The ingots were repeatedly turned over and remelted to ensure homogeneity. The compositions of alloys reported are the nominal ones since the losses during melting were negligible.

The technique and apparatus for fabricating ribbon samples with a typical cross-section of about 20 to 30 μm × 1 to 2 mm and the method of characterizing the amorphous nature of the samples by differential scanning calorimetry (DSC), X-ray and electron metallographic techniques have been described elsewhere [8]. Hardness (H_V) and tensile strength (σ_f) of as-quenched samples were measured by a Vickers microhardness tester with a 100 g load and an Instron-type tensile testing machine at a strain rate of 1.67×10^{-4} sec^{-1}, respectively. Young's modulus, Y, was determined from the slope of stress–elongation curve within the elastic limit. The density was measured by the Archimedean method using tetrabromoethane. The details for the technique are given by Shirakawa *et al.* [9]. Bend ductility testing was done for the ribbons in both the as-cast state and after 1 h anneals. Samples which were able to sustain a 180° bend were designated as being ductile. The surface structure after a 180° bend and the tensile fracture surface were observed using scanning electron microscopy. All measurements of superconducting properties T_c, $J_c(H)$ and $H_{c2}(T)$ were done resistively using a conventional four-probe technique. The critical current was defined as the threshold current at which no-zero voltage ($> 1\,\mu$V) was first detected. The temperature was measured within an accuracy of ± 0.01 K using a calibrated germanium thermometer. The magnetic field up to 9 T was applied transversely to the specimen surface and excited current.

3. Results

3.1. Formation range of the amorphous phase

The formation range of the homogeneously amorphous phase in the Zr–Nb–Si ternary system is shown in Fig. 1. The range is wide extending from 12 to 24 at% Si and the whole composition range between zirconium and niobium. No amorphous phase was found in rapidly quenched $Nb_{85}Si_{15}$ alloy even though binary $Nb_{78-83}Si_{17-22}$ alloys have been reported to exhibit an amorphous phase [8]. This indicates that completely amorphous ribbons of the zirconium-rich alloys are easier to produce than those of the niobium-rich alloys for the $(Zr–Nb)_{85}Si_{15}$ alloy series. A typical electron micrograph of the amorphous phase in the thinned $Zr_{45}Nb_{40}Si_{15}$ alloy is shown in Fig. 2, together with the selected-area diffraction pattern. The featureless contrast of the bright-field image (a) and the diffuse halos in the diffraction pattern (b) confirm the amorphous nature. No evidence of crystalline precipitates was found using dark-field electron microscopy for the alloys within the composition range described above.

It has been predicted from the transformation theories [10–12] of crystal nucleation and growth in the liquid and experimental results [13, 14] that the formation of an amorphous phase is closely related to the reduced glass temperature (T_g/T_m) (where T_g is the glass transition temperature and T_m is the melting point) and the viscosity of the alloys; that is, the larger the T_g/T_m and the higher the viscosity in the supercooled liquid, the greater is the ease of formation of the amorphous phase. In fact, the composition range in which an amorphous alloy is obtained by liquid-quenching technique is very often located around a deep eutectic in the alloy phase diagram, where T_m is the lowest. The equilibrium phase diagrams for Zr–Si [15] and Nb–Si [16] binary systems feature a eutectic reaction at the compositions of $Zr_{91}Si_9$ and $Nb_{82}Si_{18}$ having the

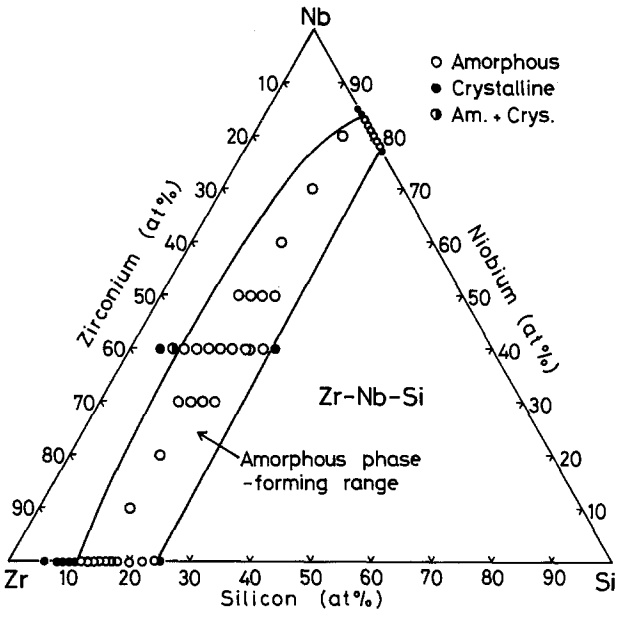

Figure 1 Composition range for the formation of an amorphous phase in the Zr–Nb–Si system.

eutectic temperatures of 1883 and 2163 K, respectively. The formation of an amorphous phase has already been reported near the eutectic composition in Zr–Si [17] and Nb–Si [8] alloys. Thus, the present amorphous phase-forming composition range also falls near the troughs of the eutectics in the Zr–Nb–Si ternary system. A similar behaviour was observed in Ti–(V, Nb or Ta)–Si [18], Zr–(V or Ta)–Si [19] and Hf–(V or Nb)–Si [5] systems. The high amorphous phase-forming tendency of alloys having compositions near a deep eutectic has been interpreted in terms of a comparatively large negative heat of formation of the liquid alloy [20]. Furthermore, the strong chemical interaction between zirconium and silicon and/or niobium and silicon is expected to yield significantly high values of T_g and viscosity, thus promoting the formation of the amorphous phase [21].

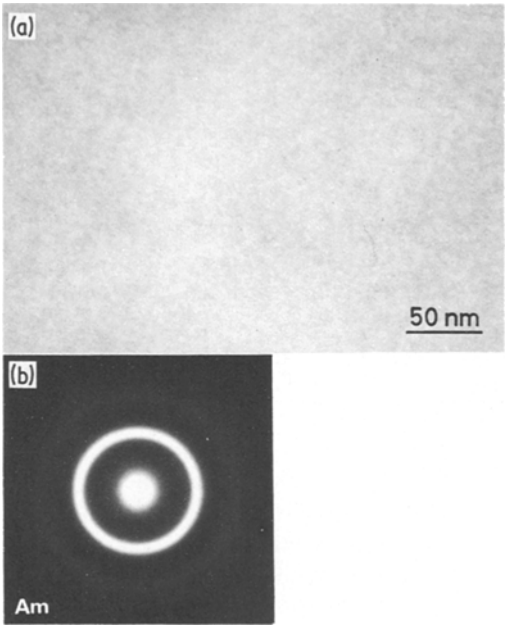

Figure 2 Transmission electron micrograph and selected-area diffraction pattern showing the as-quenched structure of $Zr_{45}Nb_{40}Si_{15}$ amorphous alloy.

3.2. Mechanical properties and thermal stability

All the amorphous alloys in Zr–Nb–Si system possess a good bend ductility. As an example, the deformation structure of $Zr_{45}Nb_{40}Si_{15}$ amorphous alloy bent completely by pressing against the edge of a razor blade is shown in Fig. 3. Numerous deformation markings can be seen near the bend edge, and no crack is observed even after such a severe deformation.

Vickers hardness, H_V, tensile fracture strength, σ_f, crystallization temperature, T_x, and the activation energy for cyrstallization, ΔE, of $Zr_{85-x}Nb_xSi_{15}$ amorphous alloys are presented in Table I. Here T_x is defined as the temperature corresponding to the start of the exothermic peak on the DSC curve measured at a heating rate of 20 K min^{-1}. ΔE is calculated by measuring the positions of the exothermic peak at different heating rates by the Kissinger method [22].

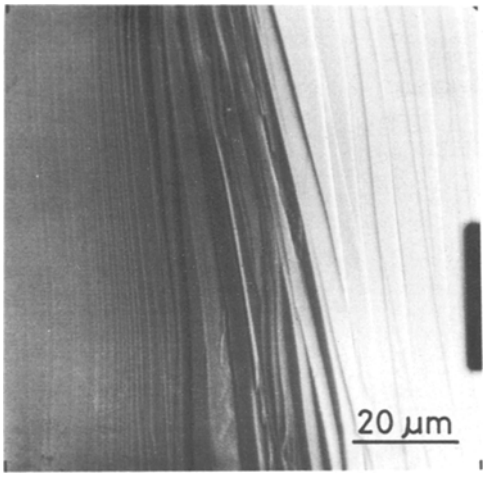

Figure 3 Scanning electron micrograph showing the deformation markings at the tip of $Zr_{45}Nb_{40}Si_{15}$ amorphous alloy bent through 180°.

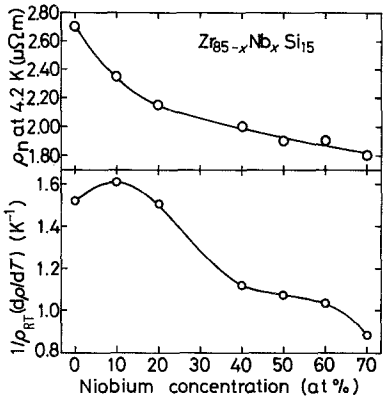

Figure 4 Niobium concentration dependences of the electrical resistivity ρ_n at 4.2 K and the temperature coefficient of resistivity (TCR) $1/\rho_{RT}$ $(d\rho/dT)$ in the temperature range 79 K to room temperature for $Zr_{85-x}Nb_xSi_{15}$ amorphous alloys.

The hardness and tensile strength increase from 420 to 690 DPN and from 1390 to 2090 MPa, respectively, with the amount of niobium. The σ_f value is almost the same level as that ($\sigma_f \simeq$ 1880 MPa) [23] for heavily cold-worked $Zr_{67}Nb_{33}$ superconducting alloy. The similar composition dependence is recognized for the T_x and ΔE. The values of T_x and ΔE increase from 759 K to a value exceeding 1000 K and from 203 to 351 kJ mol^{-1}, respectively, with increasing niobium content. Also, the critical fracture temperature is in the range 670 to 750 K. Thus, all the values of H_V, σ_f, T_x and ΔE have a similar compositional dependence against niobium content: that is, the greater the niobium content the higher are their values. The ratio H_V/σ_f (DPN/kg mm^{-2}) is almost equal to 3.0 as expected for amorphous alloys in which the indentation is accompanied with a large compressive plastic flow with little strain hardening [24]. The features of tensile fracture behaviour and fracture surface structure are the same as those of the other amorphous alloys, indicating that the fracture of the refractory metal (Zr–Nb)-based alloys proceeded by highly localized shear deformation.

3.3. Electrical resistivity

The electrical resistivity, ρ_n, at 4.2 K and the temperature coefficient of resistivity around room temperature, $1/\rho_{RT}$ $(d\rho/dT)$, for the $(Zr–Nb)_{85}Si_{15}$ amorphous alloys are plotted as a function of niobium content in Fig. 4. The resistivity significantly decreases from 2.70 to 1.80 μΩm with the substitution of niobium for zirconium. Fig. 4 also shows that all the $Zr_{85-x}Nb_xSi_{15}$ amorphous alloys exhibit a negative temperature coefficient of resistivity ranging from 1.61×10^{-4} to 0.88×10^{-4} K^{-1}, similar to the general tendency for amorphous alloys possessing the electrical resistivity above about 1.50 μΩm, and its magnitude increases with resistivity so that the zirconium-rich alloys have larger values.

TABLE I Vickers hardness, H_V, tensile fracture strength, σ_f, crystallization temperature, T_x, and the activation energy for crystallization, ΔE, for several $Zr_{85-x}Nb_xSi_{15}$ amorphous alloys

Alloys (at %)	Vickers hardness, H_V (DPN)	Tensile fracture strength, σ_f (Mpa)	Crystallization temperature, T_x (K)	Activation energy for crystallization, ΔE (kJ mol^{-1})
$Zr_{85}Si_{15}$	420	1390	759	202
$Zr_{75}Nb_{10}Si_{15}$	400	–	836	280
$Zr_{65}Nb_{20}Si_{15}$	480	–	886	330
$Zr_{55}Nb_{30}Si_{15}$	560	–	961	–
$Zr_{45}Nb_{40}Si_{15}$	620	1780	993	–
$Zr_{35}Nb_{50}Si_{15}$	650	1890	> 1000	–
$Zr_{25}Nb_{60}Si_{15}$	670	–	> 1000	–
$Zr_{15}Nb_{70}Si_{15}$	690	–	> 1000	–

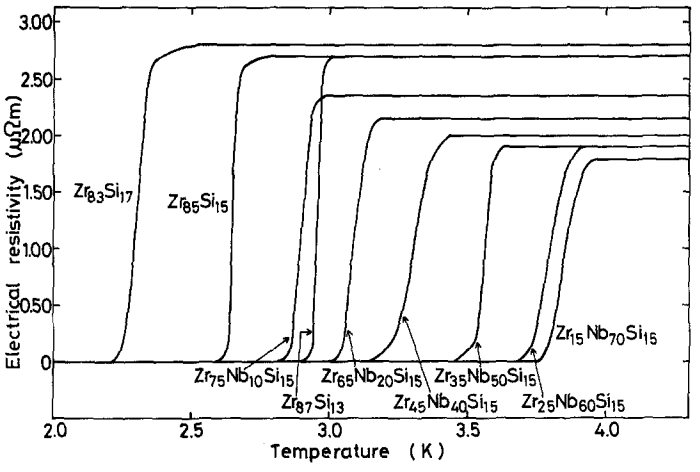

Figure 5 Electrical resistivity as a function of temperature for $Zr_{85-x}Nb_xSi_{15}$ amorphous alloys. The data of binary $Zr_{100-x}Si_x$ amorphous alloys are also represented.

3.4. Superconducting properties

Electrical resistance of $Zr_{85-x}Nb_xSi_{15}$ amorphous alloys was measured near T_c under no applied magnetic field. The result is shown in Fig. 5, wherein the data of Zr–Si amorphous alloys are also represented for comparison. The transition occurs very sharply with a temperature width of less than 0.2 K from the extremely high electrical resistivity (1.80 to 2.70 $\mu\Omega$m). Furthermore, one can see the tendency that the lower the electrical resistivity the higher is T_c. Figs 6 and 7 show the plots of T_c and ΔT_c of Zr–Nb–Si amorphous alloys as a function of niobium or silicon content. In addition, the data of Zr–M–Si (M = Ti, Hf, V, Ta, Cr, Mo or W) amorphous alloys are also represented in Fig. 6. T_c is the temperature corresponding to $R/R_n = 0.5$, where R_n is the resistance in the normal state. The transition width ΔT_c represented by a vertical bar in the figure shows the temperature interval between 0.1 and 0.9 R/R_n. As shown in Fig. 6, T_c is 2.71 K for $Zr_{85}Si_{15}$, increases with increasing niobium content and reaches 4.20 K for $Zr_5Nb_{80}Si_{15}$. On the other hand, the addition of the other transition metals results in a significant decrease in T_c even though the $Zr_{75}Ta_{10}Si_{15}$ alloy at one point exhibits a slight increase in T_c. The decrease becomes larger in the order Ta < Hf < Mo < Ti < W < V < Cr. Thus, the solute element effect on T_c of $Zr_{85-x}M_x$-Si_{15} (M = V, Nb, Ta) amorphous alloys is significantly different even in the transition metals belonging to the same group (V) of the Periodic Table. The following two factors may be responsible for such a different effect: (1) niobium element has a transition temperature much higher than those of vanadium and tantalum [25], and (2) the mixing of metal elements in different rows of the Periodic Table results in a larger decrease of T_c compared with the mixing of elements in the same transition metal series [26]. It is also

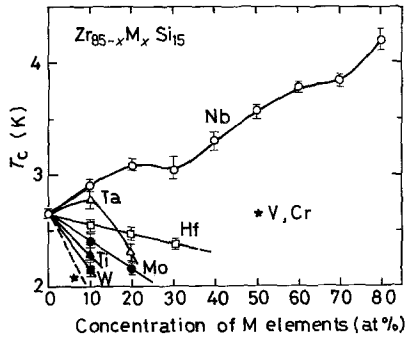

Figure 6 Niobium concentration dependences of the superconducting transition temperature, T_c, and the transition width, ΔT_c, for $Zr_{85-x}Nb_xSi_{15}$ amorphous alloys. Vertical bars represent the transition width. The data of $Zr_{85-x}M_xSi_{15}$ (M = Ti, Hf, V, Ta, Cr, Mo or W) amorphous alloys are also represented for comparison.

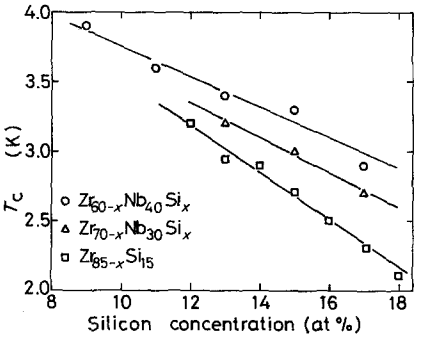

Figure 7 Silicon concentration dependence of the superconducting transition temperature, T_c, for $Zr_{100-x}Si_x$, $Zr_{70-x}Nb_{30}Si_x$ and $Zr_{60-x}Nb_{40}Si_x$ amorphous alloys.

clear in Fig. 8 that T_c varies significantly with the amount of silicon. For all the zirconium-based amorphous alloys of $Zr_{100-x}Si_x$, $Zr_{70-x}Nb_{30}Si_x$ and $Zr_{60-x}Nb_{40}Si_x$ series, T_c increases definitely with decreasing silicon content and reaches 3.2 K for $Zr_{88}Si_{12}$, 3.2 K for $Zr_{57}Nb_{30}Si_{13}$ and 3.8 K for $Zr_{51}Nb_{40}Si_9$. Disappointingly, these values are about one-half those [25] reported for conventional crystalline Zr–Nb superconducting materials. As shown in Fig. 6, the superconducting transition is somewhat broader for alloys with higher niobium content. This broadening is thought to arise from statistical fluctuations in the local niobium and zirconium concentration of the matrix because no significant structural change is observed on a spatial scale comparable to coherence length by the replacement of zirconium with niobium.

The relationship between T_c and the normal electrical resistivity, ρ_n, at 4.2 K was also investigated for the Zr–Nb–Si amorphous alloys (Fig. 8). There is a clear tendency towards the larger the electrical resistivity the lower is T_c. That is, T_c becomes lower with decreasing mean free path of electrons. Such a correlation is consistent with that [27] established for the high-resistivity crystalline superconductors.

The upper critical magnetic field, H_{c2}, was measured at various temperatures ranging from 1.5 to T_c by a standard four-probe resistance method. As an example, Fig. 9 shows the transition curves from the superconducting state to the normal state through superconducting mixed state under a current of 4×10^4 A m^{-2} at different temperatures for the $Zr_{45}Nb_{40}Si_{15}$ amorphous alloy. Resistive states are seen in a wide range of fields, following the sharp dips as the fields approach H_{c2}. The occurrence of the resistive states has been demonstrated to originate from the flux flow resistivity [28]. Here, we define H_{c2}

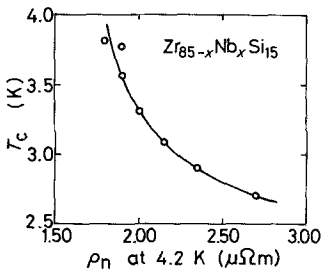

Figure 8 Relationship between T_c and electrical resistivity, ρ_n, at 4.2 K for $Zr_{85-x}Nb_xSi_{15}$ amorphous alloys.

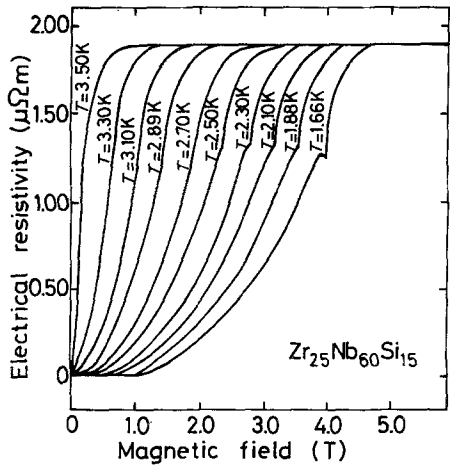

Figure 9 Electrical resistivity as a function of magnetic field at various temperatures for a $Zr_{25}Nb_{60}Si_{15}$ amorphous alloy.

to be the applied magnetic field at which the resistance of the samples begins to deviate from its normal value. The temperature dependence of H_{c2} for $Zr_{85-x}Nb_xSi_{15}$ amorphous alloys is shown in Fig. 10, wherein the solid lines represent a linear extrapolation at T_c. The H_{c2} increases linearly

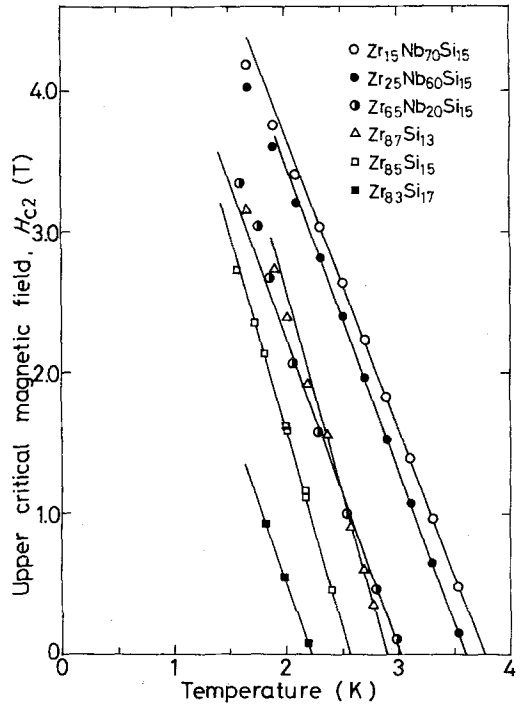

Figure 10 The upper critical magnetic field H_{c2} at various temperatures for $Zr_{85-x}Nb_xSi_{15}$ amorphous alloys. The solid lines represent a linear extrapolation at T_c. The data for binary Zr–Si amorphous alloys are also represented.

with lowering temperature over almost the whole temperature range, and the gradient at T_c, $(dH_{c2}/dT)_{Tc}$, is plotted as a function of niobium content in Fig. 11, together with the data for H_{c2} at 2.0 K. The gradient value decreases significantly with increasing niobium content, while the H_{c2} value inversely increases from 1.60 to 3.70 T with the amount of niobium. There is a clear tendency towards the higher the T_c, the higher is H_{c2}.

The critical current density, J_c, was measured at 1.45 K under an external applied magnetic field. Fig. 12 shows the critical current density, $J_c(H)$, as a function of H for $Zr_{35}Nb_{50}Si_{15}$ and $Zr_{15}Nb_{70}Si_{15}$ amorphous alloys. The value of J_c in the absence of applied field is about 2.80×10^6 A m^{-2} for $Zr_{35}Nb_{50}Si_{15}$ and 5.50×10^6 A m^{-2} for $Zr_{15}Nb_{70}Si_{15}$ and the value decreases rapidly with increasing applied field. For example, at $H = 3.5$ T, J_c is of the order of 3.0×10^5 A m^{-2} for the former alloy and 7.0×10^5 A m^{-2} for the latter alloy. Such small values of $J_c(H)$ indicate that the flux pinning force in this material is comparatively weak. This weak pinning force is considered to originate from the fact that atomic configurations in an amorphous alloy are distorted on a scale much smaller than the coherence length.

4. Discussion

4.1. Compositional dependences of electrical resistivity and its temperature coefficient

There is no established theory which provides an understanding of the magntiudes of the electrical resistivity and its temperature coefficient in the amorphous state. However, numerous experimental results [29] demonstrated that the structure, magnitude of electrical resistivity and temperature coefficient of resistivity of amorphous alloys were very similar to those of liquid alloys. Such similarities may permit us to use the theory [30] describes how the electrical resistivity of sition metal-based liquid alloys in order to understand the compositional dependences of electrical resistivity and its temperature coefficient for the $Zr_{85-x}Nb_xSi_{15}$ amorphous alloys. The theory [30] describes how the electrical resistivity of transition metal-based amorphous alloys is dominated by the concentration of solute elements, the partial structure factors among the constituent elements and the number and state of the conduction electrons in the d-state lying in the conduction band. The variation of resistivity with concentration, c, can be approximated by $\rho_n \propto c(1-c)$, indicating that a plot of resistivity behaviour against concentration is convex upwards. However, this behaviour is not consistent with the experimentally measured resistivity. Fig. 4 shows that the temperature coefficient of resistivity for the amorphous $Zr_{85-x}Nb_xSi_{15}$ alloys is negative over the entire composition range and its magnitude tends to increase with increasing resistivity. The appearance of the negative temperature coefficient (NTC) of resistivity has been qualitatively interpreted by the Faber–Ziman model [31]. This model suggests that the NTC occurs when $2K_f$ is nearly equal to K_p and/or larger than K_p, where $2K_f$ is the "spanning vector" of the Fermi surface and K_p is the position of the first maximum in the structure factor $S(k)$.

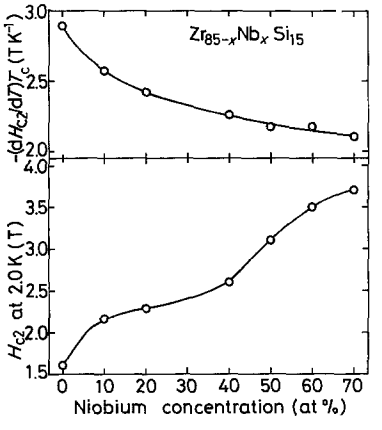

Figure 11 Niobium concentration dependences of the upper critical field gradient at T_c, $(dH_{c2}/dT)_{Tc}$, and the upper critical field at 2.0 K for $Zr_{85-x}Nb_xSi_{15}$ amorphous alloys.

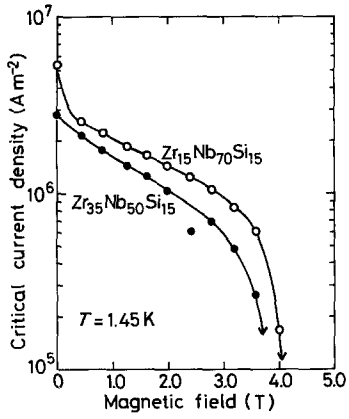

Figure 12 Critical current density, J_c, of $Zr_{35}Nb_{50}Si_{15}$ and $Zr_{15}Nb_{70}Si_{15}$ amorphous alloys as a function of magnetic field.

The broadening of the $S(k)$ peak at K_p with temperature causes the NTC. The replacement of zirconium by niobium causes the increase in the outer electron concentration per atom, resulting in a further increase of $2K_f$. As a result, the difference between $2K_f$ and K_p becomes larger with the amount of niobium. Therefore, it is inferred that the decrease in electrical resistivity by increasing the ratio of niobium to zirconium is due to the lowering of the $S(k)$ resulting from $2K_f > K_p$.

4.2. Compositional dependence of T_c

In Section 3.4, it was demonstrated that the T_c value of $(Zr–Nb)_{85}Si_{15}$ amorphous alloys rose from 2.71 to 4.20 K with increasing niobium content. The value of T_c for a strong coupling superconductor is dominated by the Debye temperature, θ_D, the electronphonon coupling constant, λ, and/or the bare density of states at the Fermi level, $N(E_f)$, and there is a close relationship whereby the larger the values of θ_D, λ and $N(E_f)$ the higher is T_c. These dominating parameters for T_c were estimated for the Zr–Nb–Si amorphous alloys in order to examine the reason for the increase in T_c on replacement of zirconium with niobium.

The coefficient of low-temperature electronic specific heat, γ, is estimated from the GLAG theory [8] using the following equation:

$$\gamma = -\frac{\pi^3}{12}\frac{k_B}{e}\frac{1}{\rho_n}\left(\frac{dH_{c2}}{dT}\right)_{T_c}. \quad (1)$$

This expression is applicable in the dirty limit where the electron mean free path is much less than the superconducting coherence length $l \ll \xi$. This criterion is well satisfied for all the $(Zr–Nb)_{85}Si_{15}$ alloys since the mean free path is estimated to be of the order of 0.5 to 1 nm from the extremely high electrical resistivity (1.80 to 2.70 $\mu\Omega$m) and the coherence length is about 7.6 nm as shown later.

λ is one of the most important dominating parameters in superconductivity and can be estimated from the McMillan equation [32],

$$\lambda = \frac{1.04 + \mu^* \ln(\theta_D/1.45T_c)}{(1 - 0.62\mu^*)\ln(\theta_D/1.45T_c) - 1.04}, \quad (2)$$

where μ^* is the Coulomb pseudopotential and the value of μ^* for the $(Zr–Nb)_{85}Si_{15}$ amorphous alloys is not known; we used $\mu^* = 0.15$, because the value lies in the range 0.1 to 0.15 for the transition metal and alloys [33]. The value of θ_D for an isotropic solid such as amorphous alloys is calculated from experimental values of Young's modulus, Y, and density, d, using the following equation [34, 35]:

$$\theta_D = \frac{h}{k_B}\left(\frac{9N}{4\pi}\right)^{1/3}\frac{Y^{1/2}}{M^{1/3}d^{1/6}}f(\nu), \quad (3)$$

where N is Avogadro's number, M is the mean atomic weight and $f(\nu)$ is a function of Poisson's ratio ν, and if ν is 0.40 commonly observed in amorphous alloys [36], $f(\nu) = 0.46$. Furthermore, $N(E_f)$ is calculated from the estimated values of γ and λ by the following expression [9]:

$$N(E_f) = \frac{1}{1+\lambda}\frac{3\gamma}{2\pi^2 k_B^2}. \quad (4)$$

The estimated values of γ, θ_D, λ and $N(E_f)$ are summarized in Table II, where the experimental values of T_c, Y and d are also shown for reference. From the values of λ ranging between about 0.63 and 0.69, the $Zr_{85}Si_{15}$ and $(Zr–Nb)_{85}Si_{15}$ amorphous alloys are concluded to be "intermediate-coupled" superconductors. The variation of T_c with replacement of zirconium by niobium is discussed on the basis of the data for θ_D, λ, γ and $N(E_f)$ shown in Table II. The values of T_c for $Zr_{85-x}Nb_xSi_{15}$ amorphous alloys are plotted against θ_D, λ, γ and $N(E_f)$ in Figs 13 and 14. A strong dependence of T_c on λ is seen and there is a clear tendency for the larger the value of λ the

TABLE II Density, d, Young's modulus, Y, superconducting transition temperature, T_c, the electronic specific heat coefficient, γ, the Debye temperature, θ_D, the electron–phonon coupling constant, λ, and the bare density of states at the Fermi level, $N(E_f)$, for several $Zr_{85-x}Nb_xSi_{15}$ amorphous alloys

Alloy (at%)	d (kg m^{-3})	Y (GN m^{-2})	T_c (K)	θ_D (K)	λ	γ (mJ mol^{-1} K^{-2})	$N(E_f)$ (states eV^{-1} atom^{-1})
$Zr_{85}Si_{15}$	6327	62.3	2.71	223	0.627	3.08	0.402
$Zr_{35}Nb_{50}Si_{15}$	7294	69.7	3.56	229	0.670	2.89	0.366
$Zr_{25}Nb_{60}Si_{15}$	7498	71.0	3.78	230	0.681	2.83	0.356
$Zr_{15}Nb_{70}Si_{15}$	7700	73.3	3.82	231	0.685	2.81	0.353

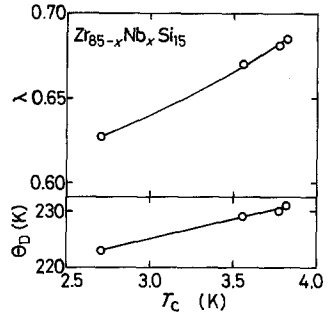

Figure 13 Relationship between T_c and the electron–phonon coupling constant, λ, and the Debye temperature, θ_D, for $Zr_{85-x}Nb_xSi_{15}$ amorphous alloys.

higher is T_c. On the other hand, $N(E_f)$, being another important parameter for T_c, decreased with niobium while T_c increased. This clearly indicates that the increase in T_c by the replacement of zirconium with niobium reflects the increase of λ:

$$\lambda = \frac{N(E_f)\langle I^2\rangle}{M\langle\omega^2\rangle}, \qquad (5)$$

where $\langle I^2\rangle$ is the squared average electron-phonon matrix element, M is the atomic mass, and $\langle\omega^2\rangle$ is the squared average phonon frequency which has approximately been estimated by θ_D^2. Such an approximation ($\langle\omega^2\rangle \simeq \theta_D^2$) is believed to be valid in the estimation of dominating parameters for the compositional dependence of T_c for the "intermediate-coupled" superconductor such as Zr–Nb–Si amorphous alloys. Considering the tendency that $N(E_f)$ decreases and the values of

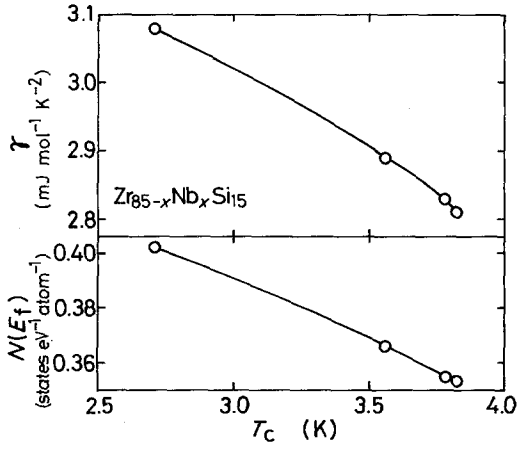

Figure 14 Relationship between T_c and the electronic specific heat coefficient, γ, and the bare density of states at the Fermi level, $N(E_f)$, for $Zr_{85-x}Nb_xSi_{15}$ amorphous alloys.

M and $\langle\omega^2\rangle \simeq \theta_D^2$ increase with niobium content, the increase in λ is thought to be a significant increase in $\langle I^2\rangle$. It is thus concluded that λ for $Zr_{85-x}Nb_xSi_{15}$ amorphous alloys is dominated by the interaction between the electron and phonon, even though the present results are in good contrast with the previous ones on amorphous $La_{80}Al_{20}$ and $La_{80}Ge_{20}$ alloys [37] that $\langle I^2\rangle/M\langle\omega^2\rangle$ is a constant and variations in λ are due to changes in $N(E_f)$.

Johnson *et al.* [38] have demonstrated that the T_c value for $(Mo–Ru)_{80}P_{20}$ amorphous alloys is in proportion to $N(E_f)$ determined from the magnetic susceptibility measurements and the decrease in T_c by the replacement of molybdenum with ruthenium is due to the decrease in $N(E_f)$. Unexpectedly, the $Zr_{85-x}Nb_xSi_{15}$ amorphous alloys have a good correlation between λ and T_c, instead of $N(E_f)$. This disagreement suggests that the dominant parameter for T_c is not always the same in both $(Mo–Ru)_{80}P_{20}$ and $(Zr–Nb)_{85}Si_{15}$ alloys in spite of being the same metal–metalloid-type amorphous superconductors.

In addition, a comparison of T_x with $N(E_f)$ as a function of niobium for $(Zr–Nb)_{85}Si_{15}$ alloys indicates a clear tendency for T_x to increase with decreasing $N(E_f)$. This tendency is consistent with the relationship between glass stability and $N(E_f)$ proposed by Nagel and Tauc [39] that in an amorphous alloy the maximum stability corresponds to the composition for which the Fermi level lies at a minimum of the density of states. The validity of the correlation has also been confirmed in metal–metal-type amorphous alloys [35].

Next, we compare the θ_D, $N(E_f)$ and λ parameters between the amorphous alloys and the crystalline zirconium or niobium metal. θ_D and $N(E_f)$ for the $(Zr–Nb)_{85}Si_{15}$ amorphous alloys are approximately 223 to 231 K and 0.353 to 0.402 states eV^{-1} atom^{-1}, respectively, lower than the weighted averages (277 to 290 K and 0.42 to 0.91 states eV^{-1} atom^{-1}) of their values of the constituent crystalline metals (zirconium and niobium) [25]. However, one can see in Fig. 15 that the value of λ is higher for the $Zr_{85}Si_{15}$ amorphous alloy than that (λ = 0.5) [25] for pure zirconium even though their values for the Zr–Nb amorphous alloys containing more than about 45 at% Nb are lower than the weighted average value of λ for the crystalline Zr–Nb alloys. It was demonstrated in Section 3.4. that the T_c of binary

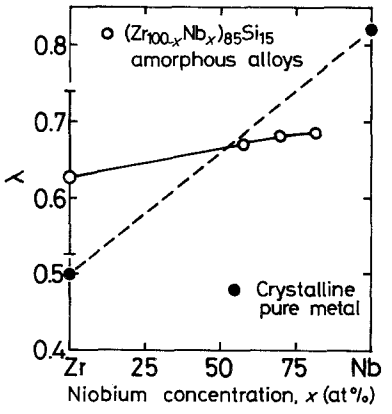

Figure 15 Niobium concentration dependences of λ for $Zr_{85-x}Nb_xSi_{15}$ amorphous alloys. The values for pure zirconium and niobium metals are also plotted for comparison.

Zr–Si amorphous alloys is higher by about three to five times than that [25] of crystalline pure zirconium, whereas the T_c of niobium-rich $(Nb–Zr)_{85}Si_{15}$ amorphous alloys is much lower than that (9.22 K) [25] of pure niobium metal. As shown in Table II, the values of $N(E_f)$ and θ_D except λ are considerably lower for the amorphous state than for the zirconium or niobium metal and alloys. On the other hand, only λ is higher for the amorphous state than for zirconium metal even though the range is limited to less than about 45 at % Nb. The compositional dependence of λ is analogous to that for T_c. This also indicates that λ more accurately reflects the T_c behaviour of the $Zr_{85-x}Nb_xSi_{15}$ amorphous alloys than did $N(E_f)$ and θ_D. Furthermore, the reason why the Zr–Si amorphous alloys exhibit a transition temperature higher than pure zirconium metal appears to be due to the high value of λ which is caused by the strong coupling between electron and phonon.

It was pointed out in Fig. 8 that there existed a close correlation between T_c and ρ_n. That is, T_c decreased with increasing ρ_n. Such a depression of T_c has been considered [40] to occur by the Pippard and Ziman condition [41, 42] on electron–phonon interactions. That is, phonons whose wavelengths exceed the electron mean free path are ineffective electron scatters and this state introduces a residual resistivity-dependent low-frequency cut-off on the phonon frequencies which contribute to T_c.

4.3. Parameters characterizing the amorphous superconductor

Some parameters characterizing the amorphous superconductors such as the GL coherence length $\xi_{GL}(0)$ at 0 K, the extrinsic GL parameter κ, the penetration depth λ_0 at 0 K, and the electronic diffusivity D, were estimated from an extended GLAG theory [9] for a "dirty" superconductor by using the following relations:

$$\xi_{GL}(0) = 1.0 \times 10^{-6} (\rho_n \gamma T_c)^{-1/2} \quad (6)$$

$$\kappa = 7.49 \times 10^3 \gamma^{1/2} \rho_n \quad (7)$$

$$\lambda_0 = 1.05 \times 10^{-2} (\rho_n / T_c)^{1/2} \quad (8)$$

$$D = \frac{4k_B c}{\pi e} \left[\frac{dH_{c2}(T)}{dT} \right]^{-1}_{T_c} \quad (9)$$

The values of their parameters for $Zr_{85-x}Nb_xSi_{15}$ amorphous alloys thus evaluated are listed in Table III together with the data of T_c, ΔT_c and ρ_n. The values of κ and λ_0 significantly decrease from 100 to 69 and from 1050 to 720 nm, respectively, with the amount of niobium, whereas D increases from 38.0 to 52.2 $mm^2\ sec^{-1}$. $\xi_{GL}(0)$ shows a nearly constant value of about 7.6 nm. The extremely high values of κ, $\xi_{GL}(0)$ and λ_0 and the low value of D appear to originate from a small value of the electron mean free path due

TABLE III Superconducting transition temperature, T_c, the transition width, ΔT_c, the electrical resistivity, ρ_n, at 4.2 K, H_{c2} gradient at T_c ($-dH_{c2}/dT$), the GL parameter, κ, the GL coherence length, $\xi_{GL}(0)$, the penetration length, λ_0, and the electronic diffisivity, D, for $Zr_{85-x}Nb_xSi_{15}$ amorphous alloys

Alloy (at%)	T_c (K)	ΔT_c (K)	ρ_n, 4.2 K ($\mu\Omega$m)	$-(dH_{c2}/dT)_{T_c}$ ($T\ K^{-1}$)	κ	$\xi_{GL}(0)$ (nm)	λ_0 (nm)	D ($mm^2\ sec^{-1}$)
$Zr_{85}Si_{15}$	2.71	0.05	2.70	2.89	100	7.6	1050	38.0
$Zr_{75}Nb_{10}Si_{15}$	2.90	0.08	2.35	2.57	87	7.8	950	42.7
$Zr_{65}Nb_{20}Si_{15}$	3.09	0.10	2.15	2.42	81	7.7	880	45.3
$Zr_{45}Nb_{40}Si_{15}$	3.30	0.20	2.00	2.26	75	7.8	820	48.5
$Zr_{35}Nb_{50}Si_{15}$	3.56	0.10	1.90	2.17	72	7.6	770	50.6
$Zr_{25}Nb_{60}Si_{15}$	3.78	0.15	1.90	2.18	72	7.4	750	50.3
$Zr_{15}Nb_{70}Si_{15}$	3.82	0.15	1.80	2.10	69	7.5	720	52.2

to the strongly disordered structure near atomic scale, evidence for which is given by the high electrical resistivities ranging from 1.80 to 2.70 $\mu\Omega$m. Therefore, it is concluded that the present $(Zr–Nb)_{85}Si_{15}$ amorphous alloys are typical type-II superconductors characterized with an extremely high degree of dirtiness. However, the degree of dirtiness is significantly decreased by the replacement of zirconium with niobium. The reason for such a difference in κ, λ_0 and D in the amorphous single-phase state is not clear and a detailed investigation of the atomic configuration in the amorphous phase will shed some light upon this problem.

4.4. Paramagnetic limitation of upper critical magnetic field

From experimentally measured values of T_c and $(dH_{c2}/dT)_{T_c}$, the so-called Maki parameters α [44, 45], the paramagnetically limited critical field $H_{c2}(0)^{**}$ [45], a maximum value of $H_{c2}(0)^{**}$ [46], the Clogston limit $H_p(0)$ [47] and the $H_{c2}{}^*(0)$ value in the absence of paramagnetic and spin-orbit scattering effects [48] are calculated using the following expressions which are applicable to dirty amorphous superconductors:

$$\alpha = 5.2758 \times 10^{-5} \left(-\frac{dH_{c2}}{dT}\right)_{T_c} \quad (10)$$

$$H_{c2}(0)^{**} = 1.31 T_c \alpha (1 + \alpha^2)^{-1/2} \quad (11)$$

$$H_{c2}(0)^{**}_{max} = 1.31 T_c \quad (12)$$

$$H_p(0) = 1.86 T_c \quad (13)$$

$$H_{c2}{}^*(0) = 0.69 T_c \left(-\frac{dH_{c2}}{dT}\right)_{T_c}. \quad (14)$$

These values thus derived are summarized in Table IV, wherein the experimentally measured H_{c2} values at 1.5 K and 50 mK and the thermodynamic critical field $H_c(0)$ at 0 K calculated from Equation 15 [49] are also shown for comparison.

$$H_c(0) = 2.44 \gamma^{1/2} T_c \quad (15)$$

As seen in the table, on replacement of zirconium with niobium, the values of $H_{c2}(0)^{**}$, $H_{c2}(0)^{**}_{max}$ and $H_p(0)$ increase, but the $H_{c2}{}^*(0)$ values remain almost unchanged. The experimental H_{c2} values at 1.5 K increase from about 3.15 to 4.78 T with the amount of niobium and hence its compositional dependence is analogous to that of $H_{c2}(0)^{**}$, $H_{c2}(0)^{**}_{max}$ and $H_p(0)$ except $H_{c2}{}^*(0)$. This result suggests that the H_{c2} values for the Zr–Nb–Si amorphous superconductors are paramagnetically limited. However, the $H_{c2}(0)$ values, which are extrapolated from the H_{c2} values measured at 1.5 and 0.05 K, are much higher than $H_{c2}(0)^{**}$ and $H_{c2}(0)^{**}_{max}$, and appear to be nearly equal to $H_p(0)$ or slightly lower than it. That is, the values of $H_{c2}(0)^{**}$ and $H_{c2}(0)^{**}_{max}$ underestimate the actual values of the critical field, indicating that the paramagnetic limitation is not so severe. This also suggests that spin-orbit scattering, which enhances the paramagnetic susceptibility of the superconducting mixed state, strongly reflects the H_{c2} value of the Zr–Nb–Si amorphous alloys. This may not be too surprising as the spin-orbit scattering effect is very strong when an alloy is made from elements having a large atomic weight and exhibits a high electrical resistivity. From the foregoing results, it is pointed out that the achievement of high values of T_c and/or ρ_n is important in order to obtain an amorphous superconductor with high critical field. Additionally, one can see in Table IV that a low value of $H_c(0)$ is caused by low transition temperature and low electronic specific heat.

5. Conclusion

Superconducting amorphous alloys having high

TABLE IV The so-called Maki parameter, α, thermodynamic critical field and various upper critical magnetic fields for $Zr_{85-x}Nb_xSi_{15}$ amorphous alloys

Alloy (at%)	α	$H_{c2}(0)^{**}$ (T)	$H_{c2}(0)^{**}_{max}$ (T)	$H_{c2}{}^*(0)$ (T)	$H_p(0)$ (T)	H_{c2} (1.5 K) (T)	H_{c2} (50×10^{-3} K) (T)	$H_c(0)$ (T)
$Zr_{85}Si_{15}$	1.49	2.88	3.55	5.17	4.93	3.15	4.62*	0.0323
$Zr_{75}Nb_{10}Si_{15}$	1.36	3.06	3.80	5.14	5.39	3.45	–	0.0350
$Zr_{65}Nb_{20}Si_{15}$	1.28	3.19	4.05	5.16	5.75	3.55	–	0.0378
$Zr_{45}Nb_{40}Si_{15}$	1.19	3.31	4.32	4.94	6.14	4.00	–	0.0404
$Zr_{35}Nb_{50}Si_{15}$	1.14	3.51	4.66	5.55	6.62	4.05	–	0.0439
$Zr_{25}Nb_{60}Si_{15}$	1.15	3.74	4.95	5.69	7.03	4.42	–	0.0467
$Zr_{15}Nb_{70}Si_{15}$	1.11	3.72	5.00	5.54	7.11	4.78	–	0.0476

*Toyota *et al.* [43].

mechanical strength as well as a highly ductile nature were found in the Zr–Nb–Si ternary system. Specimens were produced in the form of a continuous ribbon about 1 to 2 mm wide and about 0.02 to 0.03 mm thick using a melt-spinning apparatus designed for high melting point alloys. While the amorphous single phase was obtained over the whole composition range between zirconium and niobium, the silicon content was limited to the range between 12 and 24 wt%. The Vickers hardness and tensile strength increase from 420 to 690 DPN and from 1390 to 2090 MPa, respectively, with the amount of niobium. The similar compositional dependence was recognized for crystallization temperature and the activation energy for crystallization and their values increase from 759 to a value exceeding 1000 K and from 203 to 351 kJ mol^{-1}, respectively. Furthermore, these amorphous alloys were so ductile that no crack was found even after closely contacted bending. The ductility remained unchanged for 3.6×10^3 sec at temperatures below 670 K for $Zr_{65}Nb_{20}Si_{15}$ alloy. In addition, the Zr–Nb–Si alloys showed a sharp superconducting transition whose temperature increased from 2.71 to 4.20 K with increasing niobium content and with decreasing silicon content. A similar compositional dependence was also recognized for H_{c2} and the value at 2.0 K increased from 1.60 to 3.70 T. J_c for $Zr_{15}Nb_{70}Si_{15}$ alloy was as small as 5.50×10^6 A m^{-2} even at a temperature as low as 1.45 K in the absence of no applied field. The H_{c2} gradient at T_c, $(dH_{c2}/dT)_{T_c}$, and electrical resistivity, ρ_n, at 4.2 K varies from -2.89 to -2.10 T K^{-1} and 2.70 to 1.80 $\mu\Omega$m, respectively, with the amount of niobium. From comparison of the experimental measured H_{c2} values with various hypothetical H_{c2} values calculated from the Maki and the WHH theories, it was inferred that both the paramagnetic limiting and the spin-orbit scattering effects strongly reflect the actual values of the upper critical field. From the experimentally measured values of T_c, $(dH_{c2}/dT)_{T_c}$ and ρ_n, a value for γ was calculated using the GLAG theory. The γ values were used to estimate $N(E_f)$ using λ calculated from θ_D, which was determined by elastic constant and density measurements. The comparison of T_c with θ_D, λ and $N(E_f)$ as a function of niobium content indicated that λ reflects the T_c behaviour more closely than do the other parameters. The values of $\xi_{GL}(0)$ and κ were estimated to be about 7.6 nm and 69 to 100, respectively, from experimental values of $(dH_{c2}/dT)_{T_c}$ and ρ_n by using the extended GLAG theory and it was therefore concluded that the present amorphous alloys are typical soft type-II superconductors with high degree of dirtiness.

Acknowledgement

The present authors would like to thank Dr K. Shirakawa of The Research Institute of Electric and Magnetic Alloys for the density measurements.

References

1. M. TENHOVER, *Appl. Phys.* **21** (1980) 279.
2. A. INOUE, C. SURYANARAYANA, T. MASUMOTO and A. HOSHI, *Mater. Sci. Eng.* **47** (1981) 59.
3. A. INOUE, H. M. KIMURA, T. MASUMOTO, C. SURYANARAYANA and A. HOSHI, *J. Appl. Phys.* **51** (1980) 5475.
4. A. INOUE, Y. TAKAHASHI, C. SURYANARAYANA, A. HOSHI and T. MASUMOTO, *J. Mater. Sci.* **16** (1981) 3077.
5. A. INOUE, Y. TAKAHASHI, C. SURYANARAYANA and T. MASUMOTO, *ibid.* **17** (1982) 1753.
6. R. D. PARKS, (ED) "Superconductivity", Vols 1 and 2 (Marcel Dekker, New York, 1964).
7. G. BERGMANN, *Phys. Rev. B* 7 (1973) 4860.
8. T. MASUMOTO, A. INOUE, S. SAKAI, H. M. KIMURA and A. HOSHI, *Trans. Jap. Inst. Metals* 21 (1980) 115.
9. K. SHIRAKAWA, Y. WASEDA and T. MASUMOTO, *Sci. Rep. Res. Inst. Tohoku Univ.* **A-29** (1981) 229.
10. M. H. COHEN and D. TURNBULL, *Nature* **189** (1961) 131.
11. D. TURNBULL, *Contemp. Phys.* **10** (1969) 473.
12. D. R. UHLMANN, *J. Non-Cryst. Solids* 7 (1972) 337.
13. H. A. DAVIES, Proceedings of the 3rd International Conference on Rapidly Quenched Metals, Vol. 1, edited by B. Cantor, (The Metals Society, London, 1978) p. 1.
14. M. NAKA, Y. NISHI and T. MASUMOTO, *ibid.*, p. 231.
15. C. E. LUNDIN, D. J. McPHERSON and M. HANSEN, *Trans. Amer. Soc. Met.* **45** (1953) 901.
16. C. J. SMITHELLS, "Metals Reference Book", 5th edn (Butterworths, London, 1976) p. 725.
17. A. INOUE, Y. TAKAHASHI and T. MASUMOTO, *Sci. Rep. Res. Inst. Tohoku Univ.* **A-29** (1981) 296.
18. A. INOUE, H. M. KIMURA, S. SAKAI and T. MASUMOTO, Proceedings of the Fourth International Conference on Titanium, Vol. 2, edited by H. Kimura and O. Izumi, (The Metallurgical Society of AIME, Warrendale, 1980) p. 1137.
19. A. INOUE, Y. TAKAHASHI, C. SURYANARAYANA and T. MASUMOTO, *J. Mater. Sci.* submitted.
20. D. TURNBULL, *J. Physique-Colloq.* **35** (1974) 1.
21. H. S. CHEN, *Acta Metall.* **22** (1974) 897.

22. H. E. KISSINGER, *Anal. Chem.* **29** (1957) 1702.
23. C. C. KOCH and K. A. EASTON, *Cryogenics* **17** (1977) 391.
24. R. HILL, "The Mathematical Theory of Plasticity" (Oxford University Press, London, 1976) p. 213.
25. B. W. ROBERTS, Properties of Selected Superconductive Materials, 1978 Supplement, NBS Technical Note 983, US Department of Commerce, Washington, p. 12.
26. M. M. COLLVER and R. H. HAMMOND, *Phys. Rev. Lett.* **30** (1973) 92.
27. H. LUTZ, H. WEISMAN, O. F. KAMMERER and M. STRONGIN, *ibid.* **36** (1976) 1576.
28. N. TOYOTA, T. FUKASE, A. INOUE, Y. TAKAHASHI and T. MASUMOTO, *Physica* **107B** (1981) 465.
29. H. J. GÜNTHERODT and H. U. KÜNZI, "Metallic Glasses" (American Society for Metals, New York, 1978) p. 247.
30. O. DREIRACH, R. EVANS, H. J. GÜNGHERODT and H. U. KÜNZI, *J. Phys. F* **2** (1972) 709.
31. T. E. FABER and J. M. ZIMAN, *Phil. Mag.* **11** (1965) 153.
32. W. L. McMILLAN, *Phys. Rev.* **167** (1968) 331.
33. K. H. BENNEMANN and J. W. GARLAND, in "Superconductivity in d- and f-band Metals", edited by D. H. Douglass, AIP Conference Proceedings No. 4 (AIP, New York, 1972) p. 116.
34. F. H. HERBSTEIN, *Adv. Phys.* **10** (1961) 318.
35. C. C. KOCH, D. M. KROEGER, J. O. SCARBROUGH and B. C. GIESSEN, *Phys. Rev. B* **22** (1980) 5213.
36. H. S. CHEN and K. A. JACKSON, in "Metallic Glasses", edited by H. J. Leamy and J. J. Gilman (American Society for Metals, Metals Park, Ohio, 1978) p. 84.
37. K. AGYEMAN. R. MULLER and C. C. TSUEI, *Phys. Rev. B* **19** (1979) 193.
38. W. L. JOHNSON, S. J. POON, J. DURAND and P. DUWEZ, *ibid.* **18** (1978) 206.
39. S. R. NAGEL and J. TAUC, *Phys. Rev. Lett.* **35** (1975) 380.
40. L. V. MEISEL and P. J. COTE, *Phys. Rev. B* **19** (1979) 4514.
41. A. B. PIPPARD, *Phil. Mag.* **46** (1955) 1104.
42. J. M. ZIMAN, "Electrons and Phonons" (Clarendon, Oxford, 1960) Ch. 5.
43. N. TOYOTA, T. FUKASE, A. INOUE, Y. TAKAHASHI and T. MASUMOTO, unpublished research. (1981).
44. K. MAKI, *Phys.* **1** (1964) 21.
45. N. R. WERTHAMER, E. HELFAND and P. C. HOHENBERG, *Phys. Rev.* **147** (1966) 295.
46. D. DEW-HUGHES, *Rep. Prog. Phys.* **34** (1971) 821.
47. A. M. CLOGSTON, *Phys. Rev. Lett.* **9** (1962) 266.
48. R. R. HAKE, *Phys. Rev.* **158** (1967) 356.
49. B. MÜHLSCHLEGEL, *Z. Phys.* **155** (1959) 313.

Received 26 April
and accepted 28 May 1982